analytical chemistry

Article

pubs.acs.org/ac

FePt Alloy Nanoparticles for Biosensing: Enhancement of Vitamin C Sensor Performance and Selectivity by Nanoalloying

Nafiseh Moghimi and K.T. Leung*

WATLab, and Department of Chemistry, University of Waterloo, Waterloo, Ontario, Canada N2L3G1

ABSTRACT: Electrocatalytic activity of supported FePt alloy nanoparticles (NPs) with different compositions ($Fe_{25}Pt_{75}$, $Fe_{30}Pt_{70}$, $Fe_{35}Pt_{65}$) for the electro-oxidation of vitamin C is investigated. These spherical FePt NPs with nanocrystallite size of 7−9 nm are found to consist of a nanoalloy core with a more Pt-rich shell. The FePt alloy NPs are superior catalysts than Pt NPs for vitamin C electro-oxidation, with a linear concentration range of 0.01−1 mM, a high sensitivity of 4.347 mA cm^{-2} mM^{-1}, and a low detection limit of 0.1 μM (S/N = 3). By effectively reducing the overpotential for the electro-oxidation, these alloy NPs are significantly more selective to the detection of vitamin C against other common interference species, including dopamine, citric acid, uric acid, glucose, and NaCl. Enhancement in sensor performance can be attributed to the increase in surface area due to reduction of nanocrystallite size and to modification in the Pt electronic structure as a result of nanoalloying. These are supported by the X-ray diffraction data and binding energy shifts as observed by X-ray photoelectron spectroscopy, respectively. Alloying therefore represents a powerful approach to introduce synergetic properties for new biosensor applications.

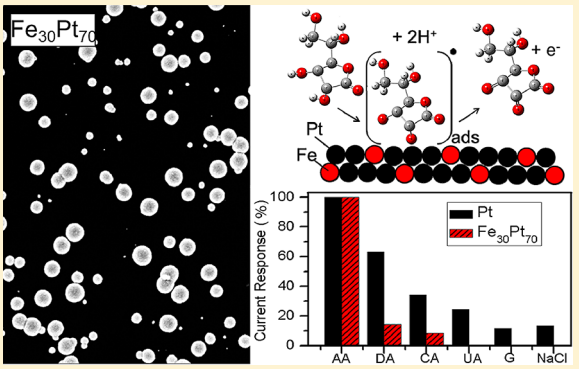

L-ascorbic acid (AA) or vitamin C is a powerful antioxidant present in food and beverages and is often used as a chemical marker for evaluating food deterioration, product quality, and freshness.[1,2] Furthermore, AA can help to promote healthy cell development, iron absorption, and normal tissue growth, which play significant roles in proper functioning of human metabolism and central nervous and renal systems.[3,4] However, overdose of AA can cause chemical conversion into oxalate, which contributes to a rise in the oxalate level of urine and results in the development of kidney stones in the long term.[5,6] Precise quantitation of AA is therefore of great importance to the food industry and human health. Several methods, including fluorometry and flow injection analysis,[7−10] spectrophotometry, and chromatography,[11−13] have been employed to detect and quantify AA in food, biological fluids, and pharmaceutical products. However, some of these methods are time-consuming, costly, or in need of specially trained operators. The UV spectrophotometric methods suffer from the interference from almost all kinds of organic compounds due to their absorption in the UV region of interest. On the other hand, visible spectrophotometric methods based on the oxidation of AA with a chromogenic redox reagent are affected by simultaneous oxidation of other phenolic antioxidants.[14] Furthermore, some of the aforementioned methods are based on the reduction properties of AA, and they are also prone to interferences by other coexisting chemicals with similar reduction properties.[15] Among these methods, the electrochemical methods have attracted much attention because of their numerous advantages, including rapid response, low cost, high sensitivity, simple-to-use and easy-to-miniaturize instrumentation, and compatibility with in vivo detection.[5,15,16]

In the electrochemical methods, AA is oxidized on bare electrodes (e.g., Pt, Au, or C), and the extent of electro-oxidation can be characterized by measuring the anodic current at the appropriate oxidation potential. However, direct electro-oxidation of AA on bare electrodes is irreversible, and it usually requires a high overpotential, which could result in electrode fouling. Furthermore, electroactive species, such as dopamine, uric acid, and glucose, are found to have oxidation potentials rather close to that of AA. As these species often coexist with AA, they introduce interference signals that cannot be easily separated.[16] To improve the selectivity of electrochemical sensors, it has been proposed that the oxidation potential of AA should be lowered by modifying the electrode with catalysts. Screening suitable catalysts with both high activity and selectivity is therefore not only of scientific significance but also beneficial to the aforementioned practical applications. Because metallic nanoparticles (NPs), especially noble metal NPs, provide a high electrochemically active surface area, they are ideal catalysts for analytes that have sluggish redox processes.[17,18] They can also act as the active component for effectively accelerating the electron transfer between the electrode and the analyte, which leads to a rapid current response and a reduced overpotential for the electrochemical reactions.[19−21] For AA detection, there are only a few studies

Received: March 15, 2013
Accepted: May 15, 2013
Published: May 15, 2013

   dx.doi.org/10.1021/ac400785h | *Anal. Chem.* 2013, 85, 5974−5980

on using noble metal films or nanostructures, including electrodes modified by Au[22−24] or Pd[15,19,25] nanostructures to obtain a more rapid response and to increase selectivity by lowering the oxidation potential of AA. However, these methods have multiple steps, and most have low sensitivity and a short linear range of detection.

Of the noble metal catalysts, Pt NPs have been extensively used in enhancement of electrochemical sensing of a variety of biomolecules,[26] including glucose,[27,28] DNA,[29] and cholestrol.[30] Numerous efforts have been devoted to the optimization of the existing Pt NP catalysts and to the design of new lower-cost catalysts with minimal Pt content by incorporating other metal components.[31−33] To date, these studies have focused primarily on fuel-cell applications[31,34,35] and none on biosensing. Of the Pt NP catalysts used for fuel-cell applications, the best efficiency has been obtained with a Pt content above 60% while noticeably poorer performance is found with a Pt content below 25%. Here, we electrochemically deposit FePt alloy NPs of different Pt content directly on the surface of the electrode, and we investigate the performance enhancement relative to Pt NPs. By keeping the Pt content near the optimal value found for catalyst applications (60−80%), we not only introduce synergistic properties due to the modification to the Pt electronic structures in this alloy NP system but also reduce material cost by employing Fe as the second metal. Our results show significant improvements in the sensitivity, detection limit, and range of linear response, higher signal-to-noise performance in neutral pH operating environment, and greatly enhanced selectivity to interference species including dopamine, uric acid, citric acid, glucose, and NaCl. This simple synthetic approach to producing bimetallic alloys can be extended to other binary metallic systems as new materials for biosensing.

2. EXPERIMENTAL DETAILS

2.1. Materials. The chemicals (all analytical grade) for the electrodeposition experiments ($FeCl_2$, H_2PtCl_6, and H_3BO_3) and for the sensing experiments (ascorbic acid, dopamine, uric acid, citric acid, glucose, and NaCl) were purchased from Sigma-Aldrich and used as received unless stated otherwise. The phosphate buffer saline solution (PBS, 0.1 M Na_2HPO_4−NaH_2PO_4−KCl, pH 7.2) was prepared from a PBS tablet (Sigma). One-side polished Si(100) wafers (p-type, B-doped, with a resistivity of 0.01−0.02 Ω·cm) were purchased from Siegert Wafer GmbH and used as substrates.

2.2. Apparatus. All electrochemical experiments were performed in a three-electrode cell workstation (CH Instruments 660A). The Si chips (15 × 2.5 mm^2, 0.4 mm thick, precut from the Si(100) wafer) were cleaned using the RCA method[36] and H-terminated by dipping in an aqueous HF (2%) solution, and they were used as the working electrode for both FePt deposition and sensor application. The as-prepared electrode was dried and stored in a N_2 atmosphere at room temperature when not in use. A standard Ag/AgCl electrode and a Pt wire were used as the reference and counter electrodes, respectively.

The surface morphology of the NPs was characterized by field-emission scanning electron microscopy (SEM) in a Zeiss Ultra Plus microscope. Crystal structures were determined by glancing-incidence X-ray diffraction (GIXRD) in a PANalytical X'Pert Pro MRD diffractometer with Cu Kα (1.542 Å) radiation at an incidence angle of 0.5°. These data are correlated with the local nanostructures and elemental compositions determined by transmission electron microscopy (TEM) in a Zeiss Libra 200MC TEM system operating at 200 kV. Chemical-state compositions of the NPs were analyzed by X-ray photoelectron spectroscopy (XPS) in a Thermo-VG Scientific ESCALab 250 microprobe with a monochromatic Al Kα X-ray source (1486.6 eV), operated with a typical energy resolution of 0.4−0.5 full width at half-maximum.

2.3. Single-Step Electrode Preparation of Pt and FePt NPs and Electrochemical Sensing. FePt alloy NPs with different compositions were prepared by potentiostatic amperometry on a Si substrate in a deoxygenated electrolyte containing 1 mM H_2PtCl_4 and 200 mM boric acid and different concentrations of $FeCl_2$. In order to obtain a homogeneous, uniform NP deposition for a particular FePt alloy composition on the H-terminated Si(100) substrate, we varied the deposition potential from −0.8 to −1.6 V (vs Ag/AgCl). Between −0.8 and −1.0 V, the resulting NPs consisted of only Pt and no Fe. At −1.1 and −1.2 V, NPs with the desired alloy composition were obtained with a uniform coverage. For potential more negative than −1.2 V, the coverage was found to be less uniform, and at −1.4 V, a black precipitate began to appear in the solution. We have therefore chosen an applied potential of −1.1 V (vs Ag/AgCl) as the deposition potential for preparing the FePt alloy NPs.

For the purpose of comparison, Pt NPs and Fe NPs were prepared using the same conditions in the same electrolyte without $FeCl_2$ and H_2PtCl_6, respectively. After the deposition, the samples were washed by filtered deionized water (18 MΩ cm) and stored in a N_2 atmosphere at room temperature until use. This method has the advantage of producing NPs with a uniform spatial distribution without agglomeration, which therefore provides the maximal exposed surface for electrocatalysis without any additional step. For electrochemical sensing using the as-prepared NP-coated electrode, cyclic voltammetry was carried out in quiescent solutions of biomolecular analyte in a PBS solution at a scan rate of 50 mV s^{-1}. Magnetic stirring was used throughout the amperometric measurements where sample injections were performed after stabilization of the baseline unless stated otherwise. The electrode was vigorously rinsed with deionized water after each measurement.

3. RESULTS AND DISCUSSION

3.1. Characterization of FePt NPs. Three different sets of FePt alloy NPs are prepared by electrodeposition for 60 s in 1 mM H_2PtCl_4 and $FeCl_2$ with three different concentrations (1, 5, and 10 mM). The SEM images shown in Figure 1 reveal spherical NPs with average sizes of 97, 102, and 107 nm, respectively, while EDX analysis shows $Fe_{25}Pt_{75}$, $Fe_{30}Pt_{70}$, and $Fe_{35}Pt_{65}$ as their respective compositions. These FePt alloy NPs all appear to have a rough surface, and they consist of grains of a few nanometers in size. Changing the deposition time from 3 to 60 s produces FePt NPs with average NP size from 10 to 100 nm, with the corresponding surface coverage increasing from 5 to 40%. The GIXRD patterns for all three samples show typical face-centered cubic (fcc) patterns of FePt alloy without any observed features corresponding to segregated Fe body-centered cubic (bcc) or Pt fcc phase. The GIXRD pattern for $Fe_{25}Pt_{75}$ NPs, shown in Figure 1, reveals small shifts in the peaks to a higher angle relative to Pt fcc. For the most intense (111) peak, the observed 0.5° shift indicates a 1.0% contraction in the fcc lattice of the $Fe_{25}Pt_{75}$ alloy NPs (from 3.911 Å for Pt fcc lattice) due to the substitution of Pt atoms with Fe atoms in

dx.doi.org/10.1021/ac400785h | Anal. Chem. 2013, 85, 5974−5980

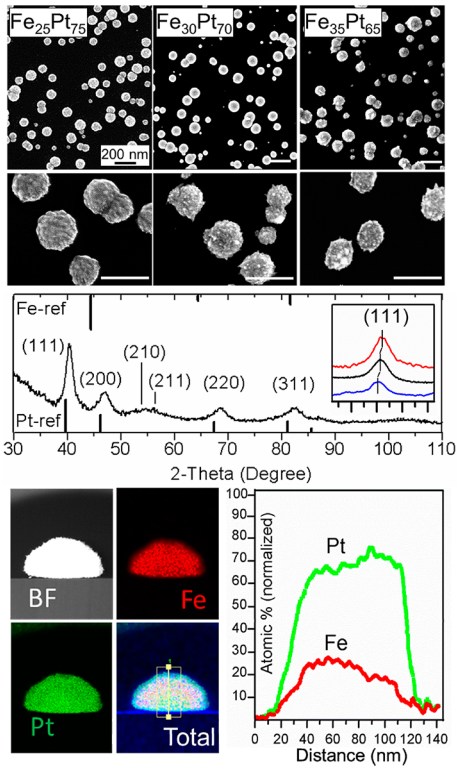

Figure 1. Top panel: SEM images of FePt alloy NPs with three different compositions, $Fe_{25}Pt_{75}$, $Fe_{30}Pt_{70}$, and $Fe_{35}Pt_{65}$, obtained from amperometry at −1.1 V vs Ag/AgCl for 60 s deposition (scale bars show 200 nm). Middle panel: Comparison of the GIXRD pattern of $Fe_{25}Pt_{75}$ alloy NPs with the reference patterns for Fe bcc (PDF2 01-085-1410) and Pt fcc (PDF2 004-0802), with the shift in the (111) peaks for $Fe_{25}Pt_{75}$, $Fe_{30}Pt_{70}$, and $Fe_{35}Pt_{65}$ NPs shown in the inset (bottom to top). Bottom panel: Bright-field (BF) STEM image of a typical $Fe_{25}Pt_{75}$ NP and its corresponding Fe and Pt EDX elemental maps and line scans along the NP (from the surface through the NP).

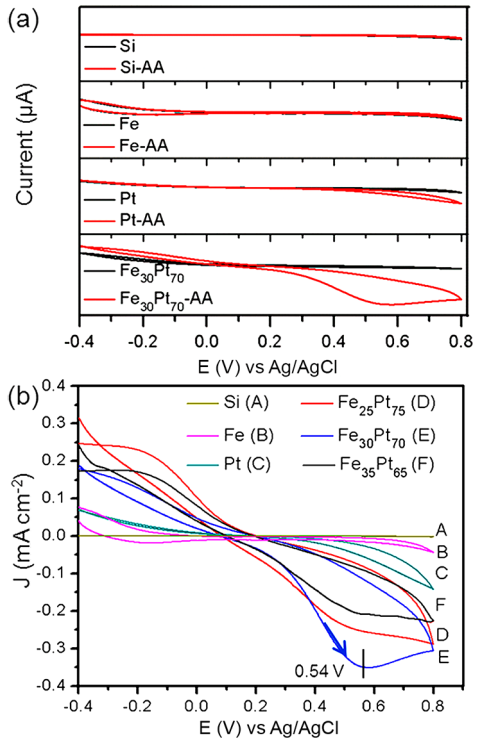

Figure 2. (a) Cyclic voltammograms of a bare Si electrode and electrodes electrodeposited with pristine Fe nanoparticles (NPs), pristine Pt NPs, and $Fe_{30}Pt_{70}$ alloy NPs, all in a 10 mM PBS solution without and with 1 mM ascorbic acid (AA). (b) Cyclic voltammograms of Si electrode, electrodes with Fe NPs, Pt NPs, and $Fe_{25}Pt_{75}$, $Fe_{30}Pt_{70}$, and $Fe_{35}Pt_{65}$ alloy NPs in a 10 mM PBS solution with 1 mM ascorbic acid (AA). Scan rate is 50 mV s^{-1}.

the cubic lattice. Similar shifts in the (111) peak by different amounts have also been observed for the $Fe_{30}Pt_{70}$ and $Fe_{35}Pt_{65}$ alloy NPs (Figure 1, inset), which indicates a respective lattice contraction of 1.2 and 1.5%. Using the widths of the respective (111) peak, we estimate the grain size to be 7, 7, and 9 nm for $Fe_{25}Pt_{75}$, $Fe_{30}Pt_{70}$, and $Fe_{35}Pt_{65}$ NPs, respectively, by the Scherrer analysis. Figure 1 also shows the STEM image of a typical $Fe_{25}Pt_{75}$ NP and its corresponding Fe and Pt elemental maps obtained by EDX analysis. The uniform distributions of both Fe and Pt elements in the elemental maps of the NP show mixed alloy NP formation, with a self-organized Pt-enriched region on the surface as indicated by the line scans throughout the NP.

3.2. Sensor Properties. To investigate the role of alloying in the electrocatalytic activities of FePt alloy NPs, we study the electro-oxidation of AA by cyclic voltammetry (CV) and potentiostatic amperometry. Figure 2a shows the CV curves acquired at a sweep rate of 50 mV s^{-1} in a solution of 10 mM PBS with and without 1 mM AA using the bare Si electrode and electrodes electrodeposited with pristine Fe NPs, pristine Pt NPs, and $Fe_{30}Pt_{70}$ alloy NPs. Evidently, the bare Si electrode and Fe NP electrode do not exhibit any current response in the presence of AA. On the other hand, the Pt NP electrode shows a discernibly stronger anodic response to the presence of AA than the Fe NP electrode but a much weaker response when compared to the alloy NP electrode. For the alloy NP electrode, the anodic peak observed at +0.54 V is attributed to the electro-oxidation of AA. Figure 2b compares the CV curves obtained in the solution of 10 mM PBS and 1 mM AA for all electrodes including those of FePt NPs with different compositions. The highest anodic peak current density (at +0.54 V) is found for the $Fe_{30}Pt_{70}$ NP electrode, with the anodic response following the order: $Fe_{30}Pt_{70}$ > $Fe_{25}Pt_{75}$ > $Fe_{35}Pt_{65}$ > Pt > Fe. Given that the $Fe_{30}Pt_{70}$ NP electrode provides the best electrocatalytic performance among the alloy and pristine NPs studied in the present work, all the subsequent tests are performed using this electrode.

In order to investigate the variation of the anodic peak current (measured at +0.54 V) with increasing AA concentration, we perform CV measurements of the $Fe_{30}Pt_{70}$ NP electrode in PBS solutions with increasing AA concentrations at a fixed sweep rate (50 mV s^{-1}), and the result is shown in Figure 3a. The anodic peak current density, J, is found to depend linearly on the AA concentration, C, in the range of 0.01 and 1 mM with a regression relation of J (mA cm^{-2}) = 0.33766 × C (mM) + 0.04538 (with a correlation coefficient of 0.9974). Furthermore, potentiostatic amperometry of the $Fe_{30}Pt_{70}$ NP electrode in PBS solutions is conducted in low AA concentrations (0.01−0.3 mM). Figure 3b shows the amperometry response of the $Fe_{30}Pt_{70}$ NP electrode at +0.5 V to successive addition of five aliquots of 5, 10, and 20 μL of 50 mM AA to a 10 mM PBS solution. After each injection, the solution is gently stirred for 1 min before the current measurement, during which the solution is kept quiescent. Evidently, successive addition of AA aliquots results in stepwise increase of anodic current. As expected, we also obtain a good

dx.doi.org/10.1021/ac400785h | Anal. Chem. 2013, 85, 5974−5980

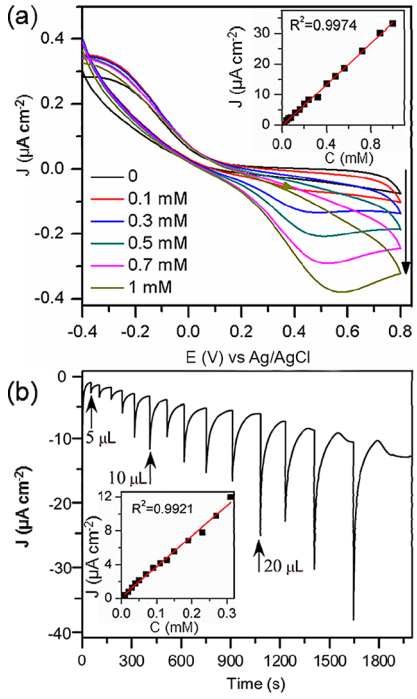

Figure 3. (a) Cyclic voltammetry of the $Fe_{30}Pt_{70}$ NP electrode (with a scan rate of 50 mV s^{-1}) in the absence and presence of different ascorbic acid (AA) concentrations in a 10 mM PBS solution. (b) Corresponding amperometric response to successive addition of five aliquots of 5, 10, and 20 μL of a stock solution of 50 mM AA to a 10 mM PBS solution. The linear relationships between the peak current density at 0.5 V and the concentration over different concentration ranges are shown in the respective insets.

linear relationship of current response to the concentration in the low concentration regime (Figure 3b, inset).

3.3. Interference Study. Coexistence of biomolecules such as dopamine, citric acid, uric acid, and glucose introduces serious interference to the electrochemical detection of AA, which hinders the practical application of the biosensor. In order to minimize the common interference signals, we employ in the present work metallic nanostructures as the catalysts in order to reduce the overpotential of AA oxidation. The current responses of $Fe_{30}Pt_{70}$ NPs to successive additions of AA are investigated using different applied potentials from 0 to 0.6 V (not shown), and the best potential (that gives the largest current response) is found to be +0.5 V (vs Ag/AgCl). However, at this potential, the common electroactive species such as dopamine and citric acid also exhibit sizable current signal similar to that for AA, indicating strong interferences toward AA determination from these biomolecules. At 30% of the value found at +0.5 V, a good current response is also obtained for AA at 0 V (vs Ag/AgCl). Amperometric responses of $Fe_{30}Pt_{70}$ NPs recorded at 0 V to successive additions of equal aliquots of AA and other biomolecules, including dopamine (DA), citric acid (CA), uric acid (UA), glucose (G), and NaCl, all with the same concentration of 20 μM, are compared with those of Pt NPs in Figure 4a. Stirring has been applied after each aliquot injection to obtain a homogeneous concentration. Both $Fe_{30}Pt_0$ NPs and Pt NPs show a notable current response to the addition of AA, with the response for $Fe_{30}Pt_0$ NPs being 3 times that for Pt NPs. Figure 4b summarizes the relative responses of both $Fe_{30}Pt_0$ NPs and Pt NPs to the additions of AA, DA, CA, UA, G, and NaCl, all normalized to the respective

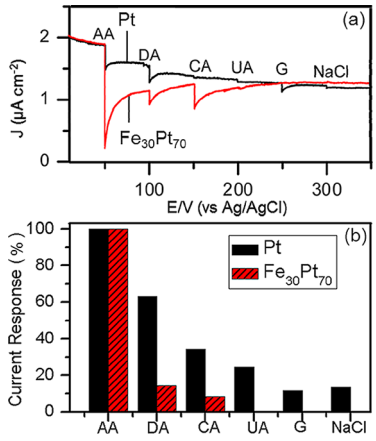

Figure 4. (a) Amperometry of $Fe_{30}Pt_{70}$ NPs and Pt NPs at an applied potential of 0 V (vs Ag/AgCl) by successive additions of 1 mM ascorbic acid (AA), dopamine (DA), citric acid (CA), uric acid (UA), glucose (G), and NaCl to 10 mM PBS to obtain a final concentration of 20 μM for all species. (b) Corresponding relative current responses normalized to the AA current response.

AA current responses. Evidently, all five species introduce current responses comparable to that of AA for Pt NPs, with the following order: DA > CA > UA > NaCl > G. In contrast, UA, G, and NaCl do not show any response for $Fe_{30}Pt_{70}$ NPs, while DA and CA only exhibit relatively weak signals (less than 15% that of AA signal). The present result therefore shows that $Fe_{30}Pt_{70}$ NPs are much more selective than Pt NPs as an AA sensor material.

3.4. Sensor Optimization. In order to obtain the best sensor performance, we increase the electroactive surface area of the electrode. This can be achieved by optimizing the NP loading onto the substrate by tuning the deposition time (to obtain the maximum NP number density) and/or increasing the surface area of the substrate (from flat Si(100) to Si nanowires). Of the FePt alloy NPs studied in the present work, the best current response to AA detection is obtained by $Fe_{30}Pt_{70}$ alloy NPs, following the order: $Fe_{30}Pt_{70}$ > $Fe_{25}Pt_{75}$ > $Fe_{35}Pt_{65}$. Using the electrolyte solution for producing the $Fe_{30}Pt_{70}$ alloy NPs at the optimized deposition potential (−1.1 V vs Ag/AgCl), we vary the deposition time from 3 to 600 s. Increasing deposition time leads to larger NPs with a higher number density (i.e., a larger surface coverage), thereby increasing the electroactive area, until a monolayer film of NPs is eventually reached at 600 s. The current response to 1 mM AA increases with increasing surface coverage and reaches a maximum at the 300 s deposition time (not shown). Further increase in the deposition time causes the merging of the NPs into a film and reducing the electroactive surface, which leads to gradual decrease in the current response. To increase the Si surface area for depositing the NPs, we prepare Si nanowires by chemical etching of the Si(100) substrate in a 5 M HF and 0.02 M $AgNO_3$ solution at room temperature for 10 min and followed by dipping in a HNO_3/H_2O (3:1) solution for 30 min (to remove the Ag deposits).[37,38] Figure 5a shows a typical morphology of the resulting Si nanowires, with significantly increased surface areas than the flat Si(100) surface. We then deposit $Fe_{30}Pt_{70}$ alloy NPs at −1.1 V (vs Ag/AgCl) for 300 s on the Si nanowires. Evidently, these alloy NPs appear to cover at least the top halves of the nanowires, as shown in Figure 5b, leading to significant increase in the NP loading on the substrate. Using the Si nanowires loaded with $Fe_{30}Pt_{70}$ NPs as

dx.doi.org/10.1021/ac400785h | Anal. Chem. 2013, 85, 5974−5980

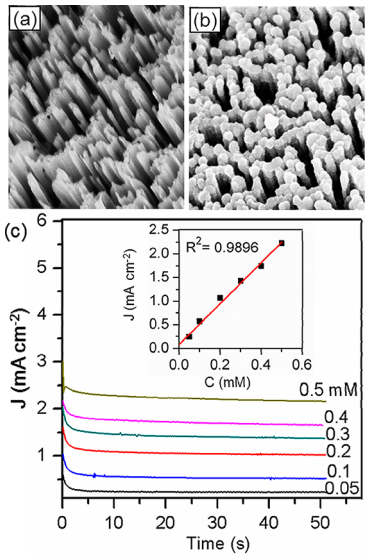

Figure 5. SEM images of Si nanowires (a) before and (b) after $Fe_{30}Pt_{70}$ NPs deposition, and (c) amperometry response of $Fe_{30}Pt_{70}$ NPs/Si nanowire electrodes in solutions with different AA concentrations (C) at an applied potential of 0 V (vs Ag/AgCl). Inset shows the linear relationship of the steady-state current density to the concentration.

the electrode, we observe over 5-fold increase in the current response, compared that found for the flat Si electrode. Furthermore, we perform amperometry for a series of solutions with different AA concentrations at 0 V (vs Ag/AgCl), at which applied potential the least interference from other species has been observed. The current density has reached a steady-state value in less than 5 s for all the solutions (Figure 5c). These steady-state current densities are found to increase linearly with increasing concentration, which provides a calibration curve for this $Fe_{30}Pt_{70}$ NPs/Si nanowire sensor (Figure 5c, inset). The sensitivity of this sensor is estimated to be 4.347 mA cm^{-2} mM^{-1}, and the detection limit of 0.1 μM is obtained by $3\sigma/S$, where σ is the standard deviation of 10 blank measurements and S is the slope of the calibration curve. The resulting sensitivity is therefore over 10 times higher than the best performance sensor materials reported to date (as summarized in Table 1), including $K_2UO_2[Fe(CN)_6]$-modified Pd/Al electrode (122.3 μA cm^{-2} mM^{-1}),[25] Pd NP composites (570 μA cm^{-2} mM^{-1}),[15] and Pd nanowires (166.5 μA cm^{-2} mM^{-1}).[19]

3.5. Electro-oxidation Model. To verify the relative near-surface composition of the FePt alloy NPs, we also analyze their chemical-state compositions by XPS after brief (20 s) Ar sputtering of the respective NP samples (to remove the carbonaceous layer due to ambient handling in air). Figure 6a compares the XPS spectra of the Fe 2p and Pt 4f regions for pristine Fe, pristine Pt, and the three FePt alloy NPs. Evidently, pristine Pt NPs and all three FePt alloy NPs exhibit Pt $4f_{7/2}$ ($4f_{5/2}$) features at essentially the same binding energy of 71.0 eV (74.3 eV), within the instrumental accuracy of 0.1 eV. For the pristine Fe NPs, two Fe $2p_{3/2}$ features at 707.0 and near 711 eV can be attributed to metallic Fe and Fe oxides, respectively. In contrast, the FePt alloy NPs all exhibit only the metallic feature at 0.4 eV higher binding energy, except for $Fe_{35}Pt_{65}$ NPs which have an additional oxide feature near 711 eV. The observed chemical shifts indicate changes in the electronic structures of the FePt alloy NPs from that of pristine Fe NPs. This is in good agreement with the in situ EXAFS data obtained for Pt alloys by Mukerjee et al.,[44] which shows more d-band vacancies for the Pt alloys than Pt metal. It should be noted that

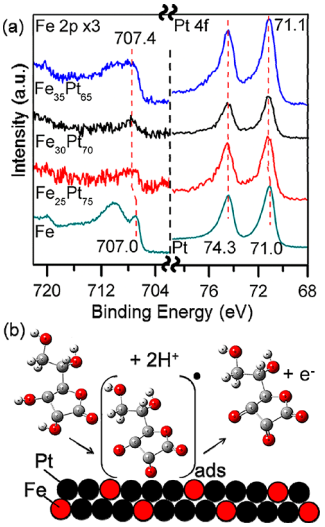

Figure 6. (a) XPS spectra of the Fe 2p and Pt 4f regions for pristine Fe, pristine Pt, and the $Fe_{25}Pt_{75}$, $Fe_{30}Pt_{70}$, and $Fe_{35}Pt_{65}$ NPs, and (b) schematic model of AA electro-oxidation on the FePt NP surface.

Table 1. Comparison of the Working Potential, Linear Range, Sensitivity and Detection Limit of the $Fe_{30}Pt_{70}$ NPs/Si Nanowire Electrodes with Other Electrodes for the Electro-oxidation of Ascorbic Acid

electrode	applied potential (V) (vs Ag/AgCl)	linear range (μM)	sensitivity (μA mM^{-1} cm^{-2})	detection limit (μM)	ref
overoxidized polypyrrole and Pd nanoparticle composites	0	1−520	570	1	15
Pd nanowires	0	25−900	166.5	0.2	19
$K_2UO_2[Fe(CN)_6]$-modified Pd/Al electrode	0.3 (SCE)	1−50	122.3	0.5	25
ferricyanide mediator/polyelectrolyte−calcium carbonate microspheres	0.27	1−2143	4.5	0.7	39
multiwall carbon nanotube−silica network−Au nanoparticles	~0.46	1000−5000	8.59	not reported	40
graphene nanosheets on pyrolyzed photoresist film	~0.35	400−6000	18.5	120	41
polyacrylic acid-coated multiwall carbon nanotubes	~−0.1	100−1000	26	49.8	42
CoNSal-modified electrode	~0.25	1−100	4.2	0.7	43
$Fe_{30}Pt_{70}$ alloy NPs on Si nanowire electrode	0	10−1000	4347	0.1	this work

dx.doi.org/10.1021/ac400785h | Anal. Chem. 2013, 85, 5974−5980

the chemical stability of the FePt NP catalysts has also been investigated by XPS before and after AA detection. No degradation or change in surface composition has been observed.

The increase in the d-band vacancies in the FePt alloy NPs has been used to account for the observed enhancement in the electroactivity of FePt alloy NPs compared to that of Pt NPs. Because Fe has more 5d vacancies than Pt, the replacement of Pt with Fe in a FePt alloy generally increases the d vacancies (relative to pristine Pt), which affects the electron affinities of the Pt atoms in the alloys. Following the mechanism of electro-oxidation of AA on the Pt electrode proposed by Casella[45] and Karabinas et al.,[46] an increase in the electron affinities of the alloy would enhance the adsorption of deprotonated AA adspecies ($C_6H_6O_6^{2-}$), which subsequently leads to oxidation of the adsorbed AA radical. Figure 6b shows a schematic diagram of the AA anionic radical formation and its adsorption to the surface of the alloy NPs. The radical then loses an electron and desorbs from the surface. Alloying is believed to increase the adsorption rate and therefore enhance the electron detection.

4. CONCLUSION

In summary, FePt alloy NPs with three different compositions have been obtained on Si substrate by electrodeposition. These NPs have been tested for electro-oxidation of AA, and all alloy compositions show higher electrocatalytic activity than pristine Pt NPs. By effectively reducing the overpotential for AA oxidation, these alloy NPs are significantly more selective to AA detection against other common interference species, including dopamine, citric acid, uric acid, glucose, and NaCl. Increasing electroactive surface area of the substrate by replacing flat Si substrate with Si nanowires enhances the current response 5-fold. Higher d vacancies of FePt relative to Pt have been used to account for the observed enhancement in the electroactivity of FePt alloy NPs. The present FePt alloy NPs can therefore provide superior sensing materials for a fast-response AA sensor with high sensitivity, wide linear detection range, and low detection limit in neutral pH operating environment.

AUTHOR INFORMATION

Corresponding Author

*E-mail: tong@uwaterloo.ca.

Notes

The authors declare no competing financial interest.

REFERENCES

(1) Gazdik, Z.; Zitka, O.; Petrlova, J.; Adam, V.; Zehnalek, J.; Horna, A.; Reznicek, V.; Beklova, M.; Kizek, R. *Sensors* **2008**, *8*, 7097−7112.
(2) Velíšek, J.; Cejpek, K. *Czech J. Food Sci.* **2006**, *25*, 49−64.
(3) Levine, M.; Downing, D. *J. Nutr. Environ. Med.* **1992**, *3*, 361.
(4) Mesías-García, M.; Guerra-Hernández, E.; García-Villanova, B. *J. Agric. Food Chem.* **2010**, *58*, 6027−6032.
(5) Qiu, S.; Gao, S.; Xie, L.; Chen, H.; Liu, Q.; Lin, Z.; Qiu, B.; Chen, G. *Analyst* **2011**, *136*, 3962−3966.
(6) Zare, H. R.; Rajabzadeh, N.; Nasirizadeh, N.; Ardakani, M. M. *J. Electroanal. Chem.* **2006**, *589*, 60−69.
(7) Ensafi, A. A.; Rezaei, B. *Anal. Lett.* **1998**, *31*, 333−342.
(8) Wu, X.; Diao, Y.; Sun, C.; Yang, J.; Wang, Y.; Sun, S. *Talanta* **2003**, *59*, 95−99.
(9) Themelis, D. G.; Tzanavaras, P. D.; Kika, F. S. *Talanta* **2001**, *55*, 127−134.
(10) Pereira, A. V.; Fatibello-Filho, O. *Anal. Chim. Acta* **1998**, *366*, 55−62.
(11) Arya, S.; Mahajan, M.; Jain, P. *Anal. Chim. Acta* **2001**, *427*, 245−251.
(12) Kall, M. A.; Andersen, C. *J. Chromatogr.. B: Biomed. Sci. Appl.* **1999**, *730*, 101−111.
(13) Lykkesfeldt, J. *Anal. Biochem.* **2000**, *282*, 89−93.
(14) Ozyürek, M.; Güçlü, K.; Bektaşoğlu, B.; Apak, R. *Anal. Chim. Acta* **2007**, *588*, 88−95.
(15) Shi, W.; Liu, C.; Song, Y.; Lin, N.; Zhou, S.; Cai, X. *Biosens. Bioelectron.* **2012**, *38*, 100−106.
(16) Xia, C.; Ning, W. *Analyst* **2011**, *136*, 288−292.
(17) Hernandez-Santos, D.; Gonzalez-Garcia, M. B.; Garcìa, A. C. *Electroanalysis* **2002**, *14*, 1225−1235.
(18) He, J. H.; Xu, Q.; Song, Z. R.; Kuang, H. Y. *Appl. Mech. Mater.* **2012**, *110−116*, 1732−1735.
(19) Wen, D.; Guo, S.; Dong, S.; Wang, E. *Biosens. Bioelectron.* **2010**, *26*, 1056−1061.
(20) Das, J.; Aziz, M. A.; Yang, H. *J. Am. Chem. Soc.* **2006**, *128*, 16022−16023.
(21) Jia, J.; Wang, B.; Wu, A.; Cheng, G.; Li, Z.; Dong, S. *Anal. Chem.* **2002**, *74*, 2217−2223.
(22) Satheesh Babu, T. G.; Varadarajan, D.; Murugan, G.; Ramachandran, T.; Nair, B. G. *J. Appl. Electrochem.* **2012**, *42*, 427−434.
(23) Morais, A.; Silveira, G.; Villis, P. C. M.; Maroneze, C. M.; Gushikem, Y.; Pissetti, F. L.; Lucho, A. M. S. *J. Solid State Electrochem.* **2012**, *16*, 2957−2966.
(24) Ghoreishi, S. M.; Behpour, M.; Saeidinejad, F. *Anal. Methods* **2012**, *4*, 2447.
(25) Pournaghi-Azar, M. Â.; Dastangoo, H.; Fadakar, R. *Electroanalysis* **2010**, *22*, 229−235.
(26) Claussen, J. C.; Kumar, A.; Jaroch, D. B.; Khawaja, M. H.; Hibbard, A. B.; Porterfield, D. M.; Fisher, T. S. *Adv. Funct. Mater.* **2012**, *22*, 3399−3405.
(27) Bo, X.; Ndamanisha, J. C.; Bai, J.; Guo, L. *Talanta* **2010**, *82*, 85−91.
(28) Su, C.; Zhang, C.; Lu, G.; Ma, C. *Electroanalysis* **2010**, *22*, 1901−1905.
(29) Zhu, N.; Chang, Z.; He, P.; Fang, Y. *Anal. Chim. Acta* **2005**, *545*, 21−26.
(30) Dey, R. S.; Raj, C. R. *J. Phys. Chem. C* **2010**, *114*, 21427−21433.
(31) Gilbert, J. A.; Kariuki, N. N.; Subbaraman, R.; Kropf, A. J.; Smith, M. C.; Holby, E. F.; Morgan, D.; Myers, D. J. *J. Am. Chem. Soc.* **2012**, 14823−14833.
(32) Wang, C.; Daimon, H.; Sun, S. *Nano Lett.* **2009**, *9*, 1493−1496.
(33) Kim, J.; Lee, Y.; Sun, S. *J. Am. Chem. Soc.* **2010**, *132*, 4996−4997.
(34) Aravind, S. S. J.; Ramaprabhu, S. *ACS Appl. Mater. Interfaces* **2012**, *4*, 3805−3810.
(35) Sheng, W.; Chen, S.; Vescovo, E.; Shao-Horn, Y. *J. Electrochem. Soc.* **2012**, *159*, B96−B103.
(36) Kern, W. *Handbook of Semiconductor Wafer Cleaning Technology*; Noyes Publications: Park Ridge, NJ, 1993.
(37) Peng, K.; Xu, Y.; Wu, Y.; Yan, Y.; Lee, S.-T.; Zhu, J. *Small* **2005**, *1*, 1062−1067.
(38) Chen, C.-Y.; Wu, C.-S.; Chou, C.-J.; Yen, T.-J. *Adv. Mater.* **2008**, *20*, 3811−3815.
(39) Li, F.; Tang, C.; Liu, S.; Ma, G. *Electrochim. Acta* **2010**, *55*, 838−843.
(40) Ragupathy, D.; Gopalan, A. I.; Lee, K.-P. *Sens. Actuators, B* **2010**, *143*, 696−703.
(41) Keeley, G. P.; O'Neill, A.; McEvoy, N.; Peltekis, N.; Coleman, J. N.; Duesberg, G. S. *J. Mater. Chem.* **2010**, *20*, 7864−7869.
(42) Huang, S.-H.; Liao, H.-H.; Chen, D.-H. *Biosens. Bioelectron.* **2010**, *25*, 2351−2355.
(43) Shahrokhian, S.; Zaremehrjardi, H. *Sens. Actuators, B* **2007**, *121*, 530−537.
(44) Mukerjee, S.; Srinivasan, S.; Soriaga, M. P.; Mcbreen, J. *J. Electrochem. Soc.* **1995**, *142*, 1409−1422.
(45) Casella, I. G. *Electroanalysis* **1996**, *8*, 128−134.

(46) Karabinas, P.; Jannakoudakis, D. *J. Electroanal. Chem.* **1984**, *160*, 159−167.

dx.doi.org/10.1021/ac400785h | *Anal. Chem.* 2013, 85, 5974−5980